Journal of Colloid and Interface Science 399 (2013) 92–98

Contents lists available at SciVerse ScienceDirect

Journal of Colloid and Interface Science

www.elsevier.com/locate/jcis

Reusable photocatalytic titanium dioxide–cellulose nanofiber films

Alexandra Snyder [a], Zhenyu Bo [a], Robert Moon [a,b,c], Jean-Christophe Rochet [d], Lia Stanciu [a,*]

[a] School of Materials Engineering, Purdue University, West Lafayette, IN, USA
[b] Birck Nanotechnology Center, Purdue University, West Lafayette, IN, USA
[c] The Forest Products Laboratory, US Forest Service, Madison, WI, USA
[d] Department of Medicinal Chemistry and Molecular Pharmacology, Purdue University, West Lafayette, IN, USA

ARTICLE INFO

Article history:
Received 12 December 2012
Accepted 22 February 2013
Available online 6 March 2013

Keywords:
Titanium dioxide
Photocatalysis
Cellulose nanofiber films
Gold
Silver
Reusable

ABSTRACT

Titanium dioxide (TiO_2) is a well-studied photocatalyst that is known to break down organic molecules upon ultraviolet (UV) irradiation. Cellulose nanofibers (CNFs) act as an attractive matrix material for the suspension of photocatalytic particles due to their desirable mechanical and optical properties. In this work, TiO_2–CNF composite films were fabricated and evaluated for photocatalytic activity under UV light and their potential to remove organic compounds from water. Subsequently, gold (Au) and silver (Ag) nanoclusters were formed on the film surfaces using simple reduction techniques. Au and Ag doped TiO_2 films showed a wider spectral range for photocatalysis and enhanced mechanical properties. Scanning electron microscopy imaging and energy dispersive X-ray spectroscopy mapping were used to evaluate changes in microstructure of the films and monitor the dispersion of the TiO_2, Au, and Ag particles. The ability of the films to degrade methylene blue (a model organic dye) in simulated sunlight has been demonstrated using UV–visible spectroscopy. Reusability and mechanical integrity of the films were also investigated.

1. Introduction

Cellulose nanomaterials (CNs) have gained considerable interest as an abundant biocompatible material with potential applications in a wide variety of fields ranging from tissue scaffolds to flexible electronics. Two general classes of CNs are cellulose nanocrystals (CNCs) and cellulose nanofibers (CNFs), both of which exhibit interesting physiochemical behavior and possess mechanical properties that are superior to bulk cellulose [1]. CNs have previously been studied as reinforcement materials for various polymer matrices [2,3], but have recently been integrated into biosensors [4], packaging [5], protective coatings [6], drug delivery systems [7], and antimicrobial films [8]. For these new functional composite systems, the individual CN particle surfaces or CN composite surfaces are functionalized with other polymers/chemicals [9], or inorganic nanoparticles [10–12]. Since, CNs are flexible, hydrophilic biopolymers that can be cast into films of different shapes and sizes, and have surfaces that are readily functionalized, they seem well suited for use as a matrix for nanoparticle dispersions [1]. Furthermore, the renewability, degradability, and non-toxicity of CN reduce concerns about negative environmental impact from the matrix material.

Titanium dioxide (TiO_2) is a well studied, stable photocatalyst capable of degradation of organic molecules via electron hole pairs that are formed upon irradiation with UV light that exceeds the material's bandgap [13]. This photocatalytic ability makes TiO_2 an ideal model material for investigating novel photocatalytic configurations. Although TiO_2 nanoparticles have been used for water decontamination applications in the past [14,15], their subsequent collection and removal is difficult. The presence of inorganic nanoparticles throughout a natural water supply or even a wastewater treatment reservoir presents concerns to human health [16,17]. Therefore a photocatalytic configuration with such nanoparticles being incorporated in a durable, biocompatible matrix has the potential to both enhance the stability of the photocatalytic nanoparticles and allow water treatment without further contamination.

Anatase, with a relatively large bandgap (~3.2 eV) is the TiO_2 phase that displays the most efficient photocatalytic activity in the UVA region of the electromagnetic spectrum (400–315 nm) [13]. Expansion of the photocatalytic properties of such particles into the visible region would lead to a more efficient use of solar energy, increasing the range of applications of TiO_2 photocatalysts. One way to increase the minimum wavelength of irradiation necessary for photocatalysis is through surface functionalization with noble metals (e.g. Au and Ag). The presence of metal nanoparticles has been shown to enhance the electron distribution and transfer on the surface of TiO_2 [18,19]. Increased charge separation between electrons and holes decreases the speed and amount of recombination, thereby facilitating enhanced oxidation of

* Corresponding author. Address: School of Materials Engineering, Neil Armstrong Hall of Engineering, 701 West Stadium Avenue, West Lafayette, IN 47907-2045, USA.
E-mail address: lstanciu@purdue.edu (L. Stanciu).

0021-9797/$ - see front matter © 2013 Elsevier Inc. All rights reserved.
http://dx.doi.org/10.1016/j.jcis.2013.02.035

molecules adsorbed on the TiO_2 [20]. Several noble metal doped TiO_2 composites have been fabricated as nanoparticle systems, but not as substrate-free supported catalyst films [18–21].

Previous studies investigated functionalization of paper [22] or regenerated cellulose [23] with TiO_2, however, this is the first study on the processing and design of photocatalytic TiO_2–CNF-based films that are usable across the entire solar spectrum. Our group previously functionalized alpha synuclein protein with nanoparticles before progressing to functionalizing biopolymer fibers. This study investigated the photocatalytic properties of CNF films that incorporated TiO_2, Au–TiO_2 and Ag–TiO_2 nanoparticles towards the decomposition of the model organic compound methylene blue (MB), which is used to examine their potential to degrade organic compounds in water.

2. Materials and methods

2.1. Materials

Titanium dioxide (anatase), methylene blue, silver nitrate, gold (III) chloride, and trisodium citrate were obtained from Sigma–Aldrich (St. Louis, MO). Cellulose nanofiber suspension (0.5 wt% CNF, 1.3 mmol COONa per g CNF, aq.) was obtained the USDA Forest Service-Forest Products Laboratory (Madison, WI). The cellulose processing followed a previously published procedure [24]; a brief description is given here. Purified Eucalyptus pulp was suspended in water containing (2,2,6,6-tetramethylpiperidin-1-yl)oxidanyl (TEMPO), sodium bromide (NaBr), sodium hydrogen carbonate ($NaHCO_3$) and sodium carbonate (Na_2CO_3). The oxidation process consisted in slowly pouring sodium hypochlorite (NaClO) at room temperature for five hours under constant mixing. After reaction completion, the TEMPO-oxidized pulp was then passed through refiners (0.1 mm and 0.05 mm gap) and microfluidizer to get a 0.5 wt% CNF suspension in water. From TEM images the CNFs were determined to be 4–20 nm in diameter. Due to the interconnected nature of the CNFs on the TEM grids, exact lengths of individual fibers were difficult to determine with observed values ranging from 200 nm to greater than 1000 nm.

2.2. Fabrication of TiO_2–CNF composite films

A stock dispersion of TiO_2 was prepared by dispersing TiO_2 nanoparticles (~21 nm, 2 g/L) in water through a combination of mechanical mixing and sonication. The TiO_2 solution (5 mL) was then mixed with as-received CNF solution (40 mL) and sonicated until well dispersed and free from agglomeration. The pH of each solution was adjusted using NaOH and HCl. Dilute aqueous solutions (1 mL) of TiO_2 and CNF were injected into the cell and zeta potential was measured using a zeta sizer nano-z, (Malvern Instruments, Westborough, MA). Electrophoretic mobility was converted to zeta potential using the Smoluchowski model. The CNF–TiO_2 mixture was then transferred to a Petri dish and dried in a controlled humidity chamber (~65% relative humidity, 25 °C) for several days until all water was removed. The resulting films had a consistent diameter of 8 cm and thickness of 30.25 μm ± 4.35.

2.3. Photodeposition of silver on TiO_2–CNF film

The dry TiO_2–CNF film was immersed in a silver nitrate solution (11.8 mM, pH 7, aq.). The system was then irradiated with UV light (~400 W) for 30 s with a noticeable change in color of the film from white to gray. The film was removed from the solution, rinsed with water, and dried overnight.

2.4. Citrate reduction of gold on TiO_2–CNF film

Trisodium citrate (8 g) was added to a gold (III) chloride solution (15 mM, pH 12, aq.). The TiO_2–CNF film was added to this solution and heated to 60 °C. After 15 min, the solution and film began to turn dark pink/purple. The reaction continued for 6 h, and then the film was rinsed with water and dried overnight. No oxidation or leaching of particles from the surface was observed visually, via UV–visible spectroscopy of the solutions, or via XPS analysis of the film surfaces.

2.5. Characterization of films

Scanning electron microscopy (SEM) and energy dispersive X-ray spectroscopy (EDS) were performed on the top surface of the films using a Philips XL40 SEM in SEI mode at 2000× magnification. No special sample preparation or coating was performed on the films in order to avoid any interference with EDS results. X-ray photoelectron spectroscopy (XPS) measurements were performed with a Kratos spectrometer. Tensile stress–strain tests were conducted using a TA Instruments Q800 Dynamic Mechanical Analyzer (DMA) used in controlled force mode, from which elastic modulus and ultimate tensile strength of CNF films were determined. The tensile tests were performed at 27 °C and 50% relative humidity using a 1.0 N/min load rate and initial pre-load of 0.005 N. Tensile specimens approximately 2 mm wide and 12 mm long (as measured by micro-caliper) were then carefully mounted onto the DMA. The lengths for determining strain were measured with calipers as the distance between DMA grips. Eight to ten tensile specimens were tested and averaged for each condition.

2.6. Photodegradation of methylene blue

The films were immersed in 25 mL of methylene blue solution (0.01 g/L, aq., initial absorbance of 1.27 ± .070) and immediately placed under the xenon arc solar simulator (Sol3A Class AAA Solar Simulator IEC/JIS/ASTM, Newport Corporation, Irvine, CA). The system was irradiated for one hour with global AM 1.5 simulated sunlight (ASTM standard spectrum) and 200 μL of solution was extracted every 5 min for analysis by UV–visible spectroscopy (Molecular Devices, Sunnyvale, CA).

3. Results and discussion

3.1. Film fabrication and optimization

Several parameters were varied to optimize the film fabrication process. The pH of the TiO_2 and CNF solutions was changed over a range of 3.5–10, and zeta potential was measured to better understand particle interactions. The CNF remained negatively charged over this entire pH range (Supplementary Fig. S1). Anatase TiO_2 has a measured isoelectric point around pH 8–8.5, with a negative surface charge occurring at pH > 8.5 [22]. The least particle agglomeration in the films was observed when mixing pH 10 CNF and TiO_2 dispersion due to electrostatic repulsion.

Resulting films displayed some TiO_2 agglomeration upon drying, but the surface distribution was good enough that the small loss of surface area did not significantly affect its photocatalytic ability. Use of surfactants limited agglomeration; however, these films showed decreased photocatalytic performance, which may be attributed to greater electron–hole recombination by the polymer surrounding the catalyst particles. Wrinkling of the films that occurred upon drying (Fig. 1) is believed to be inconsequential since the tests are performed in an aqueous environment (e.g.

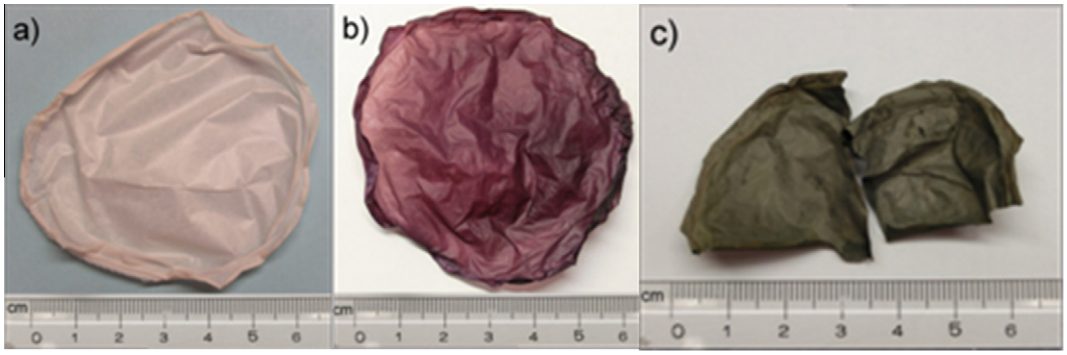

Fig. 1. Digital images of the dried TiO_2–CNF film (a), Au–TiO_2–CNF film (b), and Ag–TiO_2–CNF film (c).

methylene blue solution) and the hydrophilicity of the films allows them to smooth out in water, maximizing surface area (Supplementary Fig. S2) [25].

3.2. Photodeposition of Ag

Photoreduction of Ag under UV light is a simple, efficient method for deposition of Ag nanoparticles and nanoclusters. The surface selective formation of these particles is important for maximizing the area of contact between the catalysts and adsorbed molecules from solution. The UV irradiation time as well as the concentration and pH of the $AgNO_3$ precursor solution were varied in order to achieve full surface coverage without over-doping or completely obscuring the TiO_2. The speed of the reduction reaction was high enough to facilitate formation of Ag nanoclusters on the surface of the film in just 30–60 s irradiation time, with a noticeable color change of the film within 10 s. Irradiation time greater than 60 s led to formation of larger Ag particles in excess of what could be adsorbed onto the film, which is consistent with other reports in literature [18]. A pH value of below 5 resulted in insufficient photoreduction, with the solution changing to a pale yellow color even after several minutes under UV light.

The primary mechanism for Ag reduction in this system is believed to be the adsorption of Ag^+ ions onto the surface of the films, where Ag^+ can be reduced by excited TiO_2 photoelectrons that are transferred to the ions [26]. Cellulose has been previously used as a reducing agent in the formation of Au and Ag nanoparticles [27,28]. Based on the uniform formation of Ag on the surface of the films (Fig. 2), even in areas without TiO_2, it is probable that the CNF matrix will also contribute to the reduction of Ag^+. It has been postulated that UV irradiation of cellulose will result in cleavage of oxygen bonds between glucose monomers, leaving an aldehyde that is capable of reduction [28]. In this study, UV irradiation of CNF films (no TiO_2) in $AgNO_3$ for 30–60 s led to no observable particle formation in solution or on the films. This indicates that TiO_2 is predominately responsible for the speed and extent of Ag particle formation, with cellulose acting as a secondary reducing agent.

SEM images and EDS maps of the film surface (Fig. 2) show widespread coverage of Ag on top of the TiO_2–CNF matrix. Average size distribution of Ag indicates the presence of particles ~80 nm in diameter as well as slightly larger nanoclusters ~400 nm that formed from agglomeration of the smaller particles. While EDS mapping provided information on the location and density of Ag on the surface, the oxidation state of Ag was not apparent. XPS was used to confirm the formation of elemental Ag and rule out adsorption of $AgNO_3$ from solution. The wide scan (Fig. 3) shows Ti, O, and C peaks from the TiO_2–CNF matrix as well as strong Ag 3d peaks. The Ag 3d peaks at 360–380 eV (inset) as well as at 5 eV indicate an oxidation state of 0 for the Ag nanoclusters [20,21]. The high intensity of the Ag 3d peaks compared to the Ti 2p peak is further evidence for the extensive surface coverage observed with EDS.

3.3. Citrate reduction of Au

Although Au can be photoreduced in UV light in the same manner as Ag, the process was very susceptible to oxidation, even when nitrogen purging the reaction flasks. Instead, the citrate reduction led to more efficient particle formation and could be performed under atmospheric conditions without oxidation. In this method, the citrate acts as reducing agent, as well as a capping agent and stabilizer for the Au nanoparticles [29]. During the reduction process, the films and solution turned a dark purple color, which indicates the formation of dispersed colloidal gold [30–32].

SEM micrograph analysis indicates a bimodal distribution of Au nanoclusters, with the majority averaging ~70 nm in diameter and larger groups of particles averaging ~250 nm. EDS mapping (Fig. 4) confirms this, with several patches of higher particle density observed among a background of smaller particles that completely cover the film surface. SEM images (Fig. 4a) also show a few clusters of larger, elongated rod-like Au particles. These features were

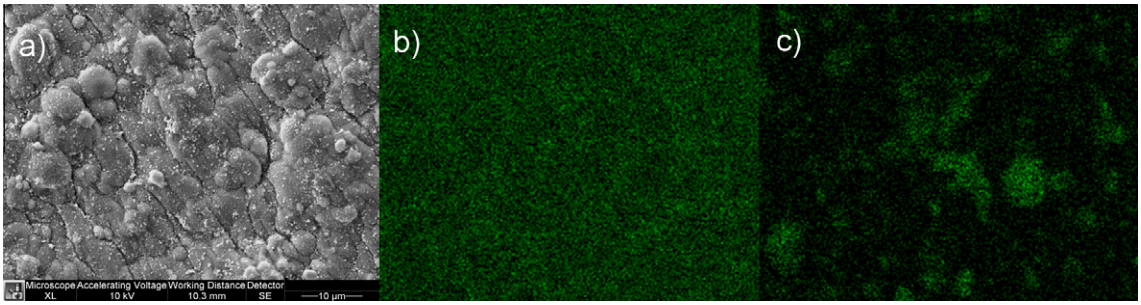

Fig. 2. SEM image (a), EDS maps – Ag (b) and Ti (c) for Ag–TiO_2–CNF film.

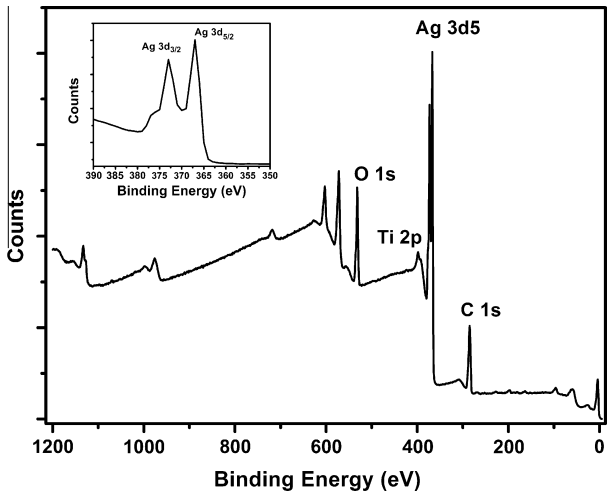

Fig. 3. Survey XPS spectrum and close-up Ag 3d peaks (inset) for Ag–TiO_2–CNF film.

rare and accounted for only a small percentage of all Au particles formed, an occurrence that has been observed with several methods of Au reduction [33].

XPS measurements confirm the presence of elemental Au on the surface (Fig. 5). The XPS wide scan shows Ti, O, and C peaks from the film matrix as well as Au4f peaks that are enlarged for the inset. These $Au4f_{5/2}$ (87 eV) and $Au4f_{7/2}$ (84 eV) are representative of zero oxidation state Au [34,35].

3.4. Photodegradation of methylene blue

The photocatalytic activity of the films under simulated sunlight was investigated using methylene blue (MB) as a model conjugated organic molecule. The MB spectrum obtained from UV–visible spectroscopy shows a strong absorbance peak around 664 nm (λ_{max}), which was used to monitor the concentration of MB. A MB control solution was irradiated for 60 min along with the TiO_2–CNF, Au–TiO_2–CNF, and Ag–TiO_2–CNF films. The irradiation of the films began immediately after they were placed in solution, with no additional time to soak. Nominal degradation was observed for the MB control, while the TiO_2–CNF films resulted in 60% degradation of the original solution concentration (Fig. 6). The Au–TiO_2–CNF, and Ag–TiO_2–CNF films performed better, resulting in 75% degradation of MB.

A steady decrease in MB concentration was observed for all of the films from 0 to 35 min of irradiation (Fig. 6). A similar, but less pronounced response was observed for films that were immersed in the MB solution but not irradiated (Fig. 7). The degree of adsorption varied between the different types of films, with Au–TiO_2–CNF films adsorbing the most MB over this time period. The speed and extent of adsorption is strongly influenced by the charge and roughness of the catalyst surface. Cationic MB molecules are known to strongly adsorb on the surface of TiO_2 via electrostatic attraction as well as interaction with surface hydroxyl groups [36]. It is considered here that more MB is adsorbed on the Au–TiO_2–CNF and Ag–TiO_2–CNF films than TiO_2–CNF films due to increased surface area, roughness, and negative charge provided by the presence of the metal nanoclusters [37]. The immediate drop in MB concentration observed for the Au–TiO_2–CNF films can be attributed to a strong Au–thiol affinity [38]. The fast, preferential MB adsorption on Au will allow more dye molecules to be in contact with the catalyst over the entire irradiation period and will contribute to the enhanced photodegradation by the Au films compared to that of the Ag films [39].

A comparison of Figs. 6 and 7 indicates that although the films with and without irradiation show similar trends in C/Co from 0 to 35 min, there is a noticeable disparity between the extent of concentration change for each group. Irradiation of the films resulted in considerably lower MB concentration, which signified that MB adsorption contributes to, but is not solely responsible for, the early concentration drop. The continuous decrease in MB concentration throughout the whole immersion period for films without irradiation indicates that adsorption is an ongoing process. However, it is likely that photodegradation begins as soon as the first layer of MB is adsorbed on the surface and the rate of degradation is subsequently limited by the extent of oxidation caused by the TiO_2 catalyst systems [36].

The same general trend in MB concentration was observed for all films after 40 min of irradiation. The rise in concentration at 40 and 50 min of irradiation (Fig. 6) may be associated with a combination of the release of desorbed MB molecules and newly formed degradation products into solution [39]. Products of the demethylation of MB, such as Azure A (λ_{max} = 625 nm) and Azure B (λ_{max} = 650 nm) [40], have chemical structures and UV–visible absorbance peaks that are similar to MB [39]. As the concentration of the degradation by-products increases in solution, there may be an additive effect on the overall absorbance values, resulting in a modest increase in C/Co. Multiple layers of MB can adsorb on top of the films, and bottom layers directly in contact with the catalysts will degrade first and desorb from the surface [41]. Any MB immobilized above the degrading layers should also be released into solution and will then need to re-adsorb, leading to a decrease in C/Co at 45 min.

Eventually, at irradiation time >50 min, the amount of available MB molecules in solution decreases, and C/Co drops steadily as determined by the amount of photodegradation occurring at the surface. The final C/Co values at 60 min are approximately 15% lower for the films functionalized with Au and Ag nanoclusters than for the films containing TiO_2 alone. The metal nanoclusters can act as electron traps that will easily accept and store electrons from excited TiO_2 [42]. The enhanced electron transfer and

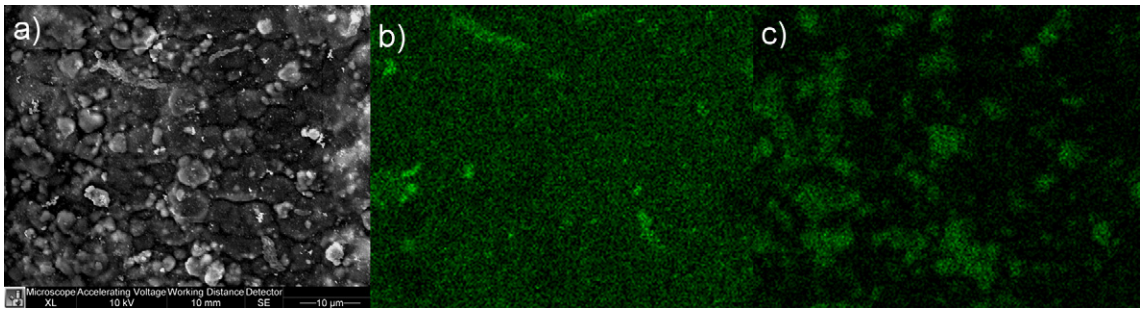

Fig. 4. SEM image (a), EDS maps – Au (b) and Ti (c) for Au–TiO_2–CNF film.

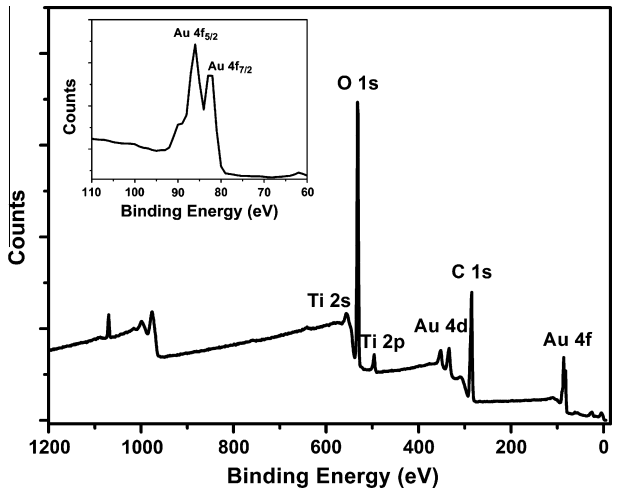

Fig. 5. XPS survey spectrum and close-up Au 4f peaks (inset) for Au–TiO_2–CNF film.

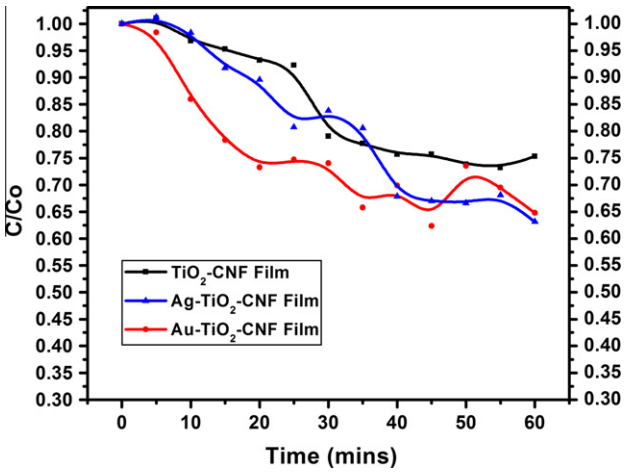

Fig. 7. Normalized C/Co of methylene blue for films that were not irradiated.

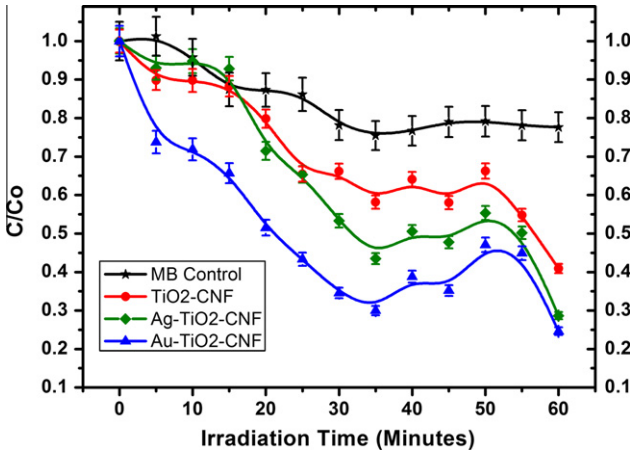

Fig. 6. Normalized C/Co of methylene blue for film irradiation in simulated sunlight, each line represents the average of four films.

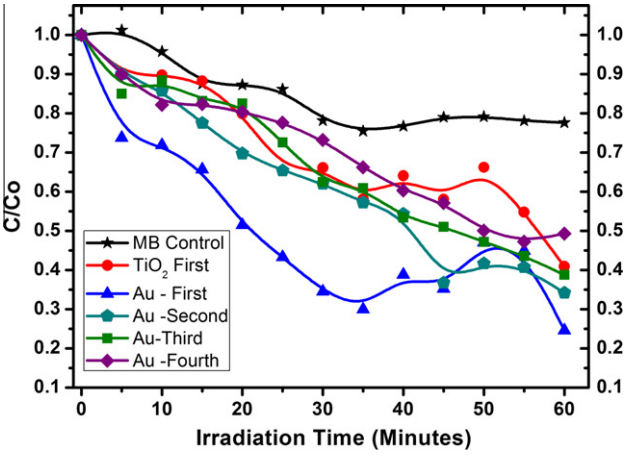

Fig. 8. Normalized C/Co of methylene blue for the reusability of Au–TiO_2–CNF films in simulated sunlight, each line represents the average of two films.

decreased electron–hole recombination contributed by Au and Ag result in superior photodegradation for these films.

3.5. Reusability and mechanical properties

A valuable feature of the Au–TiO_2–CNF and Ag–TiO_2–CNF films is their reusability without mechanical failure. After the initial hour of irradiation in MB, the films were dried overnight and the process was repeated. As anticipated, each attempt at degradation resulted in slightly higher final MB concentrations, but after four attempts the Au–TiO_2–CNF films were performing only slightly worse than the original TiO_2 films (Fig. 8). Similar results were achieved after five attempts with the Ag–TiO_2–CNF films (Fig. 9). Additionally, all of the films can be cleansed of any adsorbed dye on the surface by placing them in water under UV light or sunlight for ~10 min, which allows for more versatility in their use without worry of cross contamination.

The tensile test results for the TiO_2–CNF, Au–TiO_2–CNF and Ag–TiO_2–CNF films suggest a possible increase in elastic modulus and tensile strength as compared to the neat CNF films (Table 1). However, the TiO_2–CNF films were prone to loss of mechanical integrity after irradiation and could not consistently be reused. This could be caused by weakening of the CNF matrix by a combination of water absorption and oxidation by TiO_2. While distribution of TiO_2 throughout the matrix, along with increased hydrophilicity of the film surface limits the water absorption of the films compared to pure CNF, it cannot be completely prevented. In contrast, the Au–TiO_2–CNF and Ag–TiO_2–CNF films proved to be more durable during handling, particularly when wet.

We interpret the enhancement of the mechanical properties by the fact that conductive Au and Ag nanoclusters could divert electrons away from the matrix and distribute them more evenly throughout the MB on the surface, limiting damage to the CNF and allowing extended reusability. Tensile testing was repeated (Table 2) on the Au–TiO_2–CNF and Ag–TiO_2–CNF films after the reusability irradiation cycles were completed. TiO_2–CNF films degraded too much after one use to undergo multiple irradiation cycles or repeat tensile testing. The modulus and tensile strength decreased significantly for Au–TiO_2–CNF films after four irradiation cycles. This was likely caused by a combination of the aforementioned CNF matrix weakening and increased wear from multiple handling steps. The Ag–TiO_2–CNF films experienced a less severe decline in properties that allowed them to undergo an additional irradiation cycle (five total). Since the Ag nanoclusters were formed on film surfaces via UV photoreduction, it is possible that this process continued, to some extent, each time the films were irradiated. The ongoing reduction of Ag would help to preserve the CNF matrix and provide additional mechanical reinforcement [43,28].

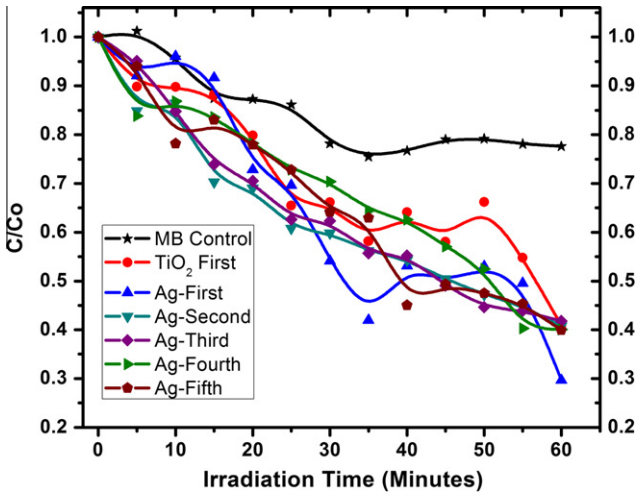

Fig. 9. Normalized C/Co of methylene blue for the reusability of Ag–TiO_2–CNF films in simulated sunlight, each line represents the average of two films.

Table 1
Average mechanical properties of the dried films, with one standard deviation.

Sample	Young's modulus (MPa)	Ultimate tensile stress (MPa)
CNF film	13.6 ± 10.4	64.6 ± 16.7
TiO_2–CNF	17.7 ± 6.6	70.7 ± 12.1
Ag–TiO_2–CNF	18.3 ± 12.8	74.5 ± 9.7
Au–TiO_2–CNF	19.9 ± 9.3	79.6 ± 11.2

Table 2
Average mechanical properties of dried films after reusability irradiation cycles were completed, with one standard deviation.

Sample	Young's modulus (MPa)	Ultimate tensile stress (MPa)
Ag–TiO_2–CNF	12.6 ± 13.7	43.3 ± 14.9
Au–TiO_2–CNF	2.0 ± 1.4	18.0 ± 6.6

Throughout the entire reusability cycle of irradiation, no noticeable mass loss or particle leaching was physically observed. In addition, the MB solutions were monitoring during irradiation using UV–visible spectroscopy. Nanoparticles of TiO_2, Ag, and Au all have characteristic UV–visible absorbance peaks that depend on particle size and concentration. Anatase TiO_2 absorbance occurs at wavelengths from 350 to 390 nm [44], Ag from 400 to 500 nm [20], and Au from 500 to 600 nm [45]. None of the spectra collected during film irradiation (Supplementary Figs. S3–S5) show any significant absorbance other than characteristic MB peaks. The lack of absorbance from 300 to 600 nm confirms the stability of nanoparticle immobilization.

4. Conclusions

Cellulose nanofiber films have a significant potential for functionalization that can offer opportunities for engineering a variety of hybrid inorganic–biological materials. Functional films with potential applications in water decontamination were produced with the incorporation of Ag, Au and TiO_2 nanoparticles with CNF. Composite films of TiO_2–CNF were shown to be strongly photocatalytically active in UV light, and subsequent modification with Au and Ag nanoclusters were shown to enhance photocatalytic efficiency in visible light. Additionally, Au and Ag modifications improved the reusability of the TiO_2–CNF films by minimizing mechanical deterioration. The photocatalytic response of Au–TiO_2–CNF and Ag–TiO_2–CNF films was reduced after multiple cycles in simulated sunlight, and eventually approached that of the TiO_2–CNF films. When considering extent of photodegradation, reusability, and mechanical integrity, the Ag–TiO_2–CNF films outperformed the rest and show potential for degradation of organic molecules in natural water sources.

Acknowledgments

The authors are grateful for the financial support offered by the U.S. Forest Service-Forest Products Laboratory (FPL). The authors thank Rick Reiner and Alan Rudie of FPL for providing materials.

Appendix A. Supplementary material

Supplementary data associated with this article can be found, in the online version, at http://dx.doi.org/10.1016/j.jcis.2013.02.035.

References

[1] R.J. Moon, A. Martini, J. Nairn, J. Simonsen, J. Youngblood, Chem. Soc. Rev. 40 (2011) 3941.
[2] M.A.S. Azizi Samir, F. Alloin, A. Dufresne, Biomacromolecules 6 (2005) 612.
[3] O.J.R.M.A. Hubbe, L.A. Lucia, M. Sain, Bioresources 3 (2008) 929.
[4] T. Zhang, W. Wang, D. Zhang, X. Zhang, Y. Ma, Y. Zhou, L. Qi, Adv. Funct. Mater. 20 (2010) 1152.
[5] H.M.C.d. Azeredo, Food Res. Int. 42 (2009) 1240.
[6] S. Eichhorn, A. Dufresne, M. Aranguren, N. Marcovich, J. Capadona, S. Rowan, C. Weder, W. Thielemans, M. Roman, S. Renneckar, W. Gindl, S. Veigel, J. Keckes, H. Yano, K. Abe, M. Nogi, A. Nakagaito, A. Mangalam, J. Simonsen, A. Benight, A. Bismarck, L. Berglund, T. Peijs, J. Mater. Sci. 45 (2010) 1.
[7] M. Roman, S. Dong, A. Hirani, W. Lee Yong, in: Polysaccharide Materials: Performance by Design, American Chemical Society, 2009, p. 81.
[8] N. Martins, C. Freire, R. Pinto, S. Fernandes, C. Pascoal Neto, A. Silvestre, J. Causio, G. Baldi, P. Sadocco, T. Trindade, Cellulose 19 (2012) 1425.
[9] K. Syverud, K. Xhanari, G. Chinga-Carrasco, Y. Yu, P. Stenius, J. Nanopart. Res. 13 (2011) 773.
[10] T. Nypelö, H. Pynnönen, M. Österberg, J. Paltakari, J. Laine, Cellulose 19 (2012) 779.
[11] S. Padalkar, J. Capadona, S. Rowan, C. Weder, R. Moon, L. Stanciu, J. Mater. Sci. 46 (2011) 5672.
[12] S. Padalkar, J.R. Capadona, S.J. Rowan, C. Weder, Y.-H. Won, L.A. Stanciu, R.J. Moon, Langmuir 26 (2010) 8497.
[13] A. Fujishima, T.N. Rao, D.A. Tryk, J Photochem. Photobiol., C 1 (2000) 1.
[14] O. Legrini, E. Oliveros, A.M. Braun, Chem. Rev. 93 (1993) 671.
[15] D.M.A. Alrousan, P.S.M. Dunlop, T.A. McMurray, J.A. Byrne, Water Res. 43 (2009) 47.
[16] T.C. Long, N. Saleh, R.D. Tilton, G.V. Lowry, B. Veronesi, Environ. Sci. Technol. 40 (2006) 4346.
[17] S.B. Lovern, J.R. Strickler, R. Klaper, Environ. Sci. Technol. 41 (2007) 4465.
[18] S.C. Chan, M.A. Barteau, Langmuir 21 (2005) 5588.
[19] M. Anpo, M. Takeuchi, J. Catal. 216 (2003) 505.
[20] L.Z. Zhang, J.C. Yu, H.Y. Yip, Q. Li, K.W. Kwong, A.W. Xu, P.K. Wong, Langmuir 19 (2003) 10372.
[21] E. Stathatos, P. Lianos, P. Falaras, A. Siokou, Langmuir 16 (2000) 2398.
[22] R. Pelton, X. Geng, M. Brook, Adv. Colloid Interface 127 (2006) 43.
[23] J. Zeng, S.L. Liu, J. Cai, L. Zhang, J. Phys. Chem. C 114 (2010) 7806.
[24] T. Saito, Y. Nishiyama, J.-L. Putaux, M. Vignon, A. Isogai, Biomacromolecules 7 (2006) 1687.
[25] Y. Tian, H. Notsu, T. Tatsuma, Photochem. Photobiol. Sci. 4 (2005) 598.
[26] M.R.V. Sahyun, N. Serpone, Langmuir 13 (1997) 5082.
[27] Z. Li, A. Friedrich, A. Taubert, J. Mater. Chem. 18 (2008) 1008.
[28] A.A. Omrani, N. Taghavinia, Appl. Surf. Sci. 258 (2012) 2373.
[29] X.H. Ji, X.N. Song, J. Li, Y.B. Bai, W.S. Yang, X.G. Peng, J. Am. Chem. Soc. 129 (2007) 13939.
[30] S. Underwood, P. Mulvaney, Langmuir 10 (1994) 3427.
[31] H.X. Li, L. Rothberg, Proc. Natl. Acad. Sci. U.S.A. 101 (2004) 14036.
[32] A.D. McFarland, C.L. Haynes, C.A. Mirkin, R.P. Van Duyne, H.A. Godwin, J. Chem. Educ. 81 (2004) 544A.
[33] J. Kimling, M. Maier, B. Okenve, V. Kotaidis, H. Ballot, A. Plech, J. Phys. Chem. B 110 (2006) 15700.
[34] J. Khanderi, R.C. Hoffmann, J. Engstler, J.J. Schneider, J. Arras, P. Claus, G. Cherkashinin, Chem. Eur. J. 16 (2010) 2300.
[35] S. Schimpf, M. Lucas, C. Mohr, U. Rodemerck, A. Brückner, J. Radnik, H. Hofmeister, P. Claus, Catal. Today 72 (2002) 63.
[36] E.A. El-Sharkawy, A.Y. Soliman, K.M. Al-Amer, J. Colloid Interface Sci. 310 (2007) 498.
[37] A. Rodríguez, J. García, G. Ovejero, M. Mestanza, J. Hazard. Mater. 172 (2009) 1311.

[38] C.D. Bain, E.B. Troughton, Y.T. Tao, J. Evall, G.M. Whitesides, R.G. Nuzzo, J. Am. Chem. Soc. 111 (1989) 321.
[39] C. Yogi, K. Kojima, N. Wada, H. Tokumoto, T. Takai, T. Mizoguchi, H. Tamiaki, Thin Solid Films 516 (2008) 5881.
[40] T. Aarthi, P. Narahari, G. Madras, J. Hazard. Mater. 149 (2007) 725.
[41] R. Yuan, R. Guan, W. Shen, J. Zheng, J. Colloid Interface Sci. 282 (2005) 87.
[42] T. Hirakawa, P.V. Kamat, J. Am. Chem. Soc. 127 (2005) 3928.
[43] E. Fortunati, I. Armentano, Q. Zhou, A. Iannoni, E. Saino, L. Visai, L.A. Berglund, J.M. Kenny, Carbohydr. Polym. 87 (2012) 1596.
[44] C.-C. Weng, K.-H. Wei, Chem. Mater. 15 (2003) 2936.
[45] S. Link, M.A. El-Sayed, J. Phys. Chem. B 103 (1999) 8410.